Scientific Annals, School of Geology, Aristotle University of Thessaloniki Proceedings of the XIX CBGA Congress, Thessaloniki, Greece	Special volume 99	323-332	Thessaloniki 2010

Fe-Mn NODULAR CONCRETIONS ASSOCIATED WITH MIDDLE JURASSIC OCEANIC MELANGE (ARGOLIS, GREECE)

Photiades A.D.

Institute of Geology and Mineral Exploration, Olympic Village, 13677 Acharnae, Attica, Greece, fotiadis@igme.gr

Abstract: Fe-Mn nodular concretions from Angelokastron and Lykotroupi areas, Northern Argolis Greece, are friable and compact types. They are associated with Middle Jurassic radiolarian red chert and red siliceous shale matrix slivers, originated and detached from a Middle Jurassic oceanic mélange. Friable Mn concretions consist of poly- or mononucleate nodules lacking primary botryoidal microstructures and possessing a unique composition. They form by the replacement of chalcedonic jasper by cryptomelane and todorokite; these concretionary crystalline manganese-structures are dissected by a birnessite phase oxidized to ntsutite and then crosscut by veinlets of hollandite and manganiferous carbonated fluroapatite during late-stage hydrothermal alteration. The resultant composition consists mostly of manganese with a very low content of iron and transition metals. The mineralogical and chemical compositions differ from those of recent or fossil manganese nodules and are related to a hydrothermal field. Compact Fe-Mn concretions consist of jasper and chert dissected by veinlets of hydrothermal todorokite. Sulphides with magnetite characterize these concretions, even when altered and silicified. Some enclose scattered fragments of magnesiochromite with Ni-rich todorokite as veinlets and as concretionary crystalline structures. Some others, such as silicified basaltic fragments, contain remnants of copper mineralization such as sulfides, oxides, and hydroxide copper minerals, generated by an older hydrothermal event with subsequent oxidation. Furthermore, a few compact concretions, which were chemically treated, revealed that they contain equal amounts of iron and manganese similar to the hydrothermal ferromanganiferous crusts on basalts. The reworked Fe-Mn nodular concretions resulted from submarine hydrothermal and fissural activity. These processes took place during the pre-emplacement period of an oceanic crust unit preserved today as the Subpelagonian ophiolite.

Keywords: SEM, chemical analysis, Fe-Mn concretions, hydrothermal, oceanic melange, Argolis.

1. Introduction

In this paper, we present a study on iron-manganese nodular concretions being described for the first time from tectonically disrupted Middle Jurassic cherts of the ophiolites of Northern Argolis, Greece. Geological data together with various laboratory investigations on the Fe-Mn concretions have been conducted in order to decode their mineralogical and chemical distribution and place limitations on their origin that are useful in discerning the tectonic history on their host assemblages. Manganiferous concretions with Ni-rich todorokite and carbonate-fluorapatite which replace and cross-cut the various silicified nodular rocks and the radiolarian Jurassic cherts were also found in Angelokastron locality and have already been studied (Photiades et al., 1995; Perseil et al., 1998).

2. Geological setting of the Fe-Mn concretions

In Angelokastron and Lykotroupi localities of Northern Argolis (Fig.1), the siliceous shale, chert and jasper associated with iron and manganese concretions are presently sandwiched below a northwest-vergent Eocene thrust of Upper Triassic limestone and over the Triassic-Jurassic shallow-water carbonate platform. Besides, the footwall carbonate platform is topped by compacted pelagic limestone of Middle Jurassic age, topped by Upper Jurassic cherts (Baumgartner, 1985) that grade upsection into Upper Jurassic ophiolite-derived detrical sequences bearing MORB and clasts with boninitic affinities (Photiades, 1986; Capedri et al., 1996).

New radiolarian biochronological analyses have revealed that most of the iron-manganese concretions contain a Liassic radiolarian chert nucleus. They are interpreted as being reworked nodular iron-manganese concretions exclusively associated with Middle Jurassic age radiolarian red chert and

red siliceous shale matrix slivers, originating and being detached from a Middle Jurassic oceanic melange (Chiari et al., 2003, 2004a, 2006). However, the adjacent surfaced pillow-lava nappe with a mid-ocean ridge basalt affinity (Dostal et al., 1991; Saccani et al., 2003) bearing Fe-Cu-stockwork and Mn-ore (Photiades 1986) is exclusively topped by an Upper Triassic (Carnian to Norian) radiolarian red chert succession (Bortolotti et al., 2001, 2002, 2003; Chiari et al. 2004b, 2007).

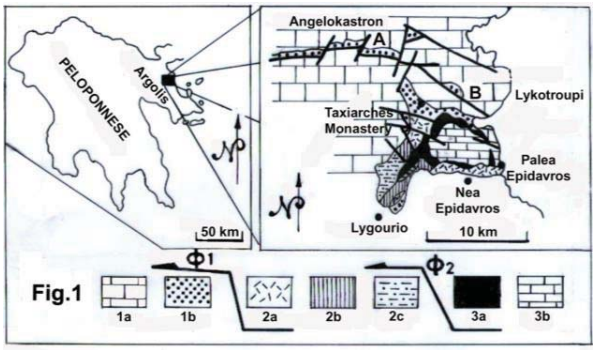

Fig. 1. Geological simplified map of Northern Argolis with Angelokastron (A) and Lykotroupi (B) localities (modified from Photiades, 1986). Triassic-Jurassic shallow-water limestone (1a), ophiolitic melange of Malm age (1b), pillow-lava ophiolite nappe (2a), Meso-autochthonous series with Cretaceous - Lower Eocene carbonate succession (2b), post-Ypresian flysch (2c), serpentinite melange (3a) with Upper Cretaceous limestone (3b), Φ1: late Jurassic tectonic phase and Φ2: late Eocene tectonic phase.

The pillow-lava nappe of Argolis and the Middle Jurassic oceanic melange slivers were emplaced onto the Pelagonian platform in Late Jurassic time and were involved again in thrusting during the Late Eocene (Photiades 1986; Capedri et al., 1996).

The chert and siliceous shale matrix slivers of Angelokastron and Lykotroupi localities (Fig.2), are up to 10m thick, in shades of various colors ranging from reddish brown to dark brown, are completely tectonically isolated, isoclinal folded (Fig. 3A, B), sheared and fractured indicating the effects of intense tectonic phases. Within this siliceous thin-bedded, soft and fine textured shale matrix, various more competent nodular or conglomerate breccias are irregularly associated such as serpentinite, basalt, chert, and jasper and are mixed with iron-manganese nodular concretions. Matrix and nodular concretions are fractured and are generally filled with quartz, chalcedony and calcite.

The iron and manganese nodular concretions show variable size from 5 to 35cm in diameter (Fig. 3C, D). The degree of mineralization was found to be from poor to rich. This character is clearly shown in the field with differences with respect to color, hardness, and texture and compactness. More mineralized nodular concretions were darker in color, fine in texture, loose and were easy to sample.

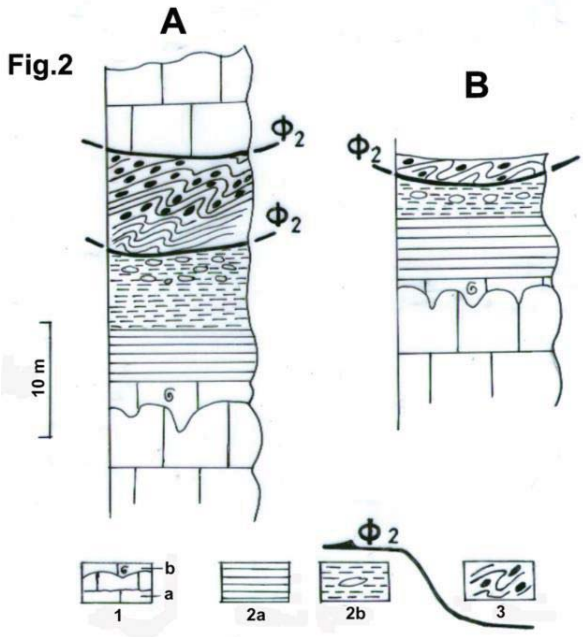

Fig. 2. Geological logs of Angelokastron (A) and Lykotroupi (B) with Fe-Mn nodular concretion outcrops. Triassic-Jurassic shallow-water limestone (1a) with condensed pelagic limestone of Middle Jurassic age (1b), Upper Jurassic cherts (2a), Upper Jurassic ophiolite-derived detrical sequence (2b), Middle Jurassic oceanic melange bearing Fe-Mn nodular concretions (3), and Φ2: late Eocene tectonic phase.

3. Morphology

Most of the iron-manganese concretions range in shape from sub-angular to ellipsoidal and include some potato-shaped nodules with rugged rinds (Fig. 3). Larger nodules are commonly fragmented. Some expose irregular rugged surfaces suggestive of irregular nuclei and some others present smooth and granular surfaces. Most concretions are black with sub-metallic lustre. Figure 3A exemplifies a mononucleate nodule with chert nucleus; figure 3B shows a polynucleate nodule. All of the polynucleate nodules (e.g., Fig. 3C) have nuclei or fractured substratum of chalcedonic jasper concentrated at their bottoms revealing in some way the original lithological oceanic floor, at the time of their growth.

Similar to the concretions described above there are massive, compact and very dense nodular to

sub-angular types lacking nuclei and have smooth and rough to granular surfaces too; these pertain to the altered remnants of basalt (Fig. 3D), serpentinite, silicified rocks, chert and jasper.

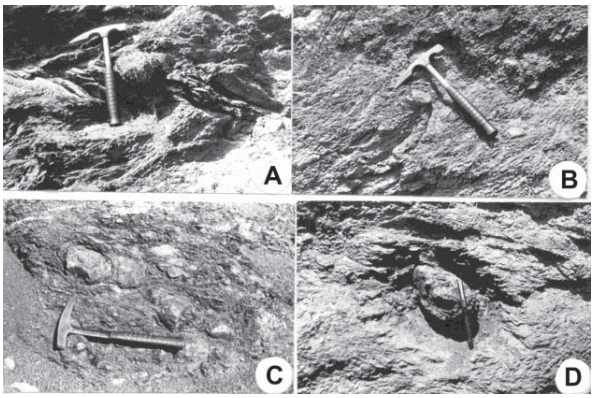

Fig. 3. Angelokastron (A) and Lykotroupi (B) with the tightly folded and sheared Middle Jurassic cherts and red siliceous shale matrix, bearing respectively various sizes of Fe-Mn nodular concretions (C and D).

4. Methods

Microscopic examination of polished thin sections were made under transmitted and reflected light, and selected samples were further analyzed by reflectance spectroscopy, scanning electron microscopy (SEM) and back-scattered electron imaging (BSE). Mineral analyses were made by X-ray diffraction (XRD), infra-red (IR) spectroscopy, and microchemical analyses by electron-microprobe techniques (CAMEBAX of the Museum National d'Histoire Naturelle of Paris). Chemical analyses were made by atomic absorption spectroscopy for Si, Mn, Fe, Al, Ni, Co and Cu.

5. Mineralogy

Reflected light and SEM analysis of the nodular concretions revealed two basic types: **(i) friable concretions** (Fig.3B) which contain nuclei of slightly crystallized spherical masses composed of spherulitic growth structures of fibrous chalcedony, as confirmed by the 555cm^{-1} band in infra-red spectrum observation (e.g. Badia and Frohlich, 1975); **(ii) massive or compact** concretions of mineralized jasper, chert, altered and silicified rocks, and basaltic fragments (Fig. 3D).

5.1. Friable concretions

Friable concretions from Angelokastron locality (as demonstrated by samples A4, A5, A7, A8, A11, A15, A16, A22, A64, A70 and A72) are related to nodular yellowish or red chalcedony jasper.

The dominant manganese mineral of these concretions is an intermediate member of the **cryptomelane series** ($K_{1-2}Mn_8O_{16}xH_2O$). Cryptomelane is developed by a concretionary weakly crystalline structure, under weak reflectance and anisotropy (with more grey color on the figure 5A) and progressively evolves into minute grains with more crystalline structure that is underlined by higher anisotropy. The cores of these concretionary cryptomelane crystalline structures (Fig. 5A) are nearly isotropic; infrared spectra show that the cores contain a silico-aluminous compound.

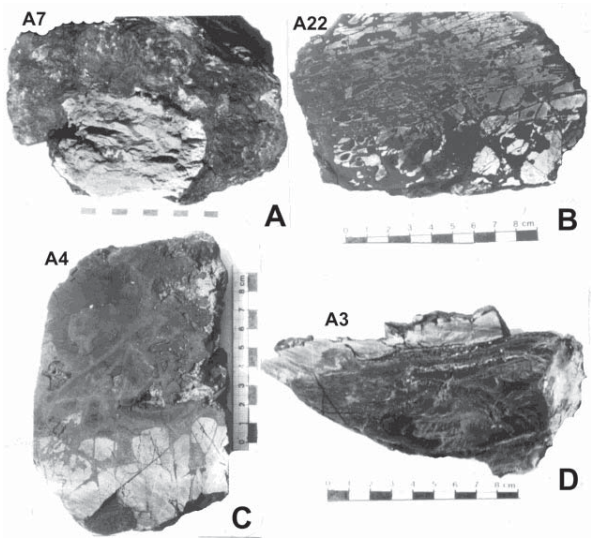

Fig. 4. Typical sections of Fe-Mn nodular concretions. A: Mononucleate concretion; B: Polynucleate; C: Polynucleate concretion. All nuclei are composed of chalcedonic jasper; D: nodular silicified basalt bearing sulphide mineralization.

Microprobe analyses (Tab.1) demonstrate a homogeneous composition, where iron is low, Na and K very nearly the same. Co and Cu are prominent among trace elements (Tab. 2).

A jasper sample (A24) includes **hollandite** ($[Ba, K]_{1-2}Mn_8O_{16}xH_2O$), the most barium rich member, but free of Fe (Tab.3), of the cryptomelane series; the hollandite occurs as veinlets dissecting a well-crystallized **todorokite** ($[Na,Ca,Mn]_2Mn_5O_{12}3H_2O$) matrix. The todorokite matrix has a sheaf-like texture (Fig. 5B) comparable to that in veinlets described from the Alps (Perseil and Latouche, 1989).

Furthermore, the largest part of concretionary cryptomelane crystalline structures is dissected by fine-veinlets of **birnessite** ($[Ca,Na]\ Mn_7O_{14}3H_2O$).

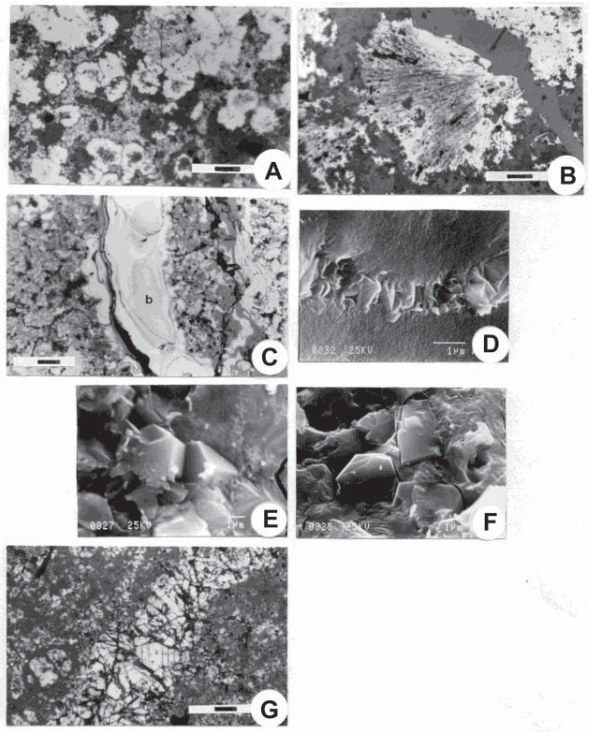

Fig. 5. Various Mn-oxides in friable concretions. **A:** Concretionary cryptomelane showing grey central part areas formed by silico-aluminous compound with copper and cobalt in poor traces. (A15 sample, natural reflected light, scale 30 μm); **B:** Crystal of todorokite revealing sheaf-like microstructure that participated as concretion into the jaspers. (natural reflected light; scale 30 μm); **C:** Birnessite (b) under the process of nsutite oxidation, particular in proximity to the microfractures (natural reflected light; 30 μm); **D, E, F:** crystallized fluorapatite in very fine-veinlets, developed in slightly crystallized birnessite. (A8 sample, SEM microphotographs); **G:** Well crystallized pyrolusite in the concretion (A14 sample, natural reflected light; scale 30 μm).

The presence of birnessite (7Å manganate) was confirmed by X-ray diffraction (strong peaks at 7.2 and 1.4 Å, moderate at 3.6 Å, and weak at 2.445 and 1.4 Å), and by infrared analysis (spectra in the regions of 3600 cm^{-1} and 600 - 400 cm^{-1}). Very often, the birnessite of these concretions oxygenizes in **nsutite** [$(Mn^{4+}, Mn^{2+})(O, OH)_2$] (Fig. 5C) indicative of an increase in oxygen fugacity.

Table 1. Representative microprobe analysis of cryptomelane (A8-A15 samples).

	MnO_2	Fe_2O_3	K_2O	Na_2O	BaO	SrO	Σ
1	94.83	0.06	4.04	0.42	-	0.15	95.50
2	93.80	0.11	4.16	0.41	-	0.10	98.68
3	94.45	1.54	3.41	0.62	-	-	100.02
4	94.83	1.35	3.46	0.62	-	-	100.26
5	94.97	0.72	3.62	0.33	-	-	99.64

Table 2. Representative microprobe analysis of cryptomelane trace elements (A 4 sample).

	As	Sb	Co	Cu	Ni	Pb	Zn
1	73	181	312	450	30	793	216
2	73	186	346	590	145	187	238
3	72	128	311	545	107	262	210
4	71	158	273	476	82	123	165

The majority of the studied concretions contain fine-veinlets of **manganiferous carbonated-fluorapatite** (Fig.5D, Tab.4); these veinlets represent the relatively youngest generation of fissures. They are crystallized (Fig. 5E, F), hydrated, and contain 2 to 3.33 wt% fluorine. Infrared spectra show an absorption band in the 3μm region.

One somewhat spongy textured friable concretion includes **manganite** (MnOOH) in a pyrolusite matrix (sample A1). **Pyrolusite** (MnO_2) is also the most important matrix constituent in several other concretions (notably in sample A14, Fig. 5G).

On the other hand, the friable concretions from Lykotroupi locality are related to red-chert nodular concretions (as demonstrated by samples B5, B6, B7, B8 and B9), and are characterized by largely crystallized **pyrolusite** (B5) crosscut by numerous fine-veinlets (up to 20μm thick) of **cryptomelane** and **todorokite**. The cryptomelane contains iron, K and Si (Tab. 5) and epigenetically replaces the radiolarians, the todorokite revealing a decrease of barium content (Tab. 5). In addition, it is noted that all samples are dissected by chalcedony and calcite veinlets, where calcite developed to manganiferous calcite.

Finally, the paragenetic evolution of the friable Mn concretions is marked by the successive presence and evolutionary crystallinity of cryptomelane, by highly crystallized todorokite and by manganite that occupies the same paragenetic order than cryptomelane and todorokite and evolved into pyrolusite. While hollandite and birnessite that oxidizes into nsutite, they are entirely associated with mineralogical evolution in late fissures. However, the manganiferous carbonated-fluorapatite in fine veinlets represent the youngest generation.

5.2. Compact concretions

Compact concretions of Angelokastron locality predominate over those from Lykotroupi locality and are together mineralogically more heterogeneous than friable Mn concretions. The oxides of compact concretions occur disseminated within a jasper host (as in samples A17, A18, A21), or in

Table 3. Representative microprobe analysis of hollandite.

	MnO_2	Fe_2O_3	Al_2O_3	TiO_2	PbO	CoO	CuO	NiO	ZnO	SiO_2	CaO	MgO	K_2O	Na_2O	BaO	SrO	Σ
1	77.90	0.05	0.28	0.06	-	0.17	0.17	-	-	0.64	0.88	0.27	0.01	0.03	16.15	-	96.61
2	78.21	-	0.29	-	-	0.25	0.04	-	-	0.59	1.49	0.23	0.06	-	15.35	0.08	96.51
3	78.45	-	0.26	0.06	-	0.23	-	0.01	-	0.65	0.83	0.19	0.03	0.04	17.10	0.04	97.89
4	78.52	0.10	0.29	-	-	0.28	0.51	-	-	0.55	1.38	0.37	0.01	0.07	13.02	0.04	95.14
5	78.64	-	0.33	-	-	0.16	0.33	-	-	0.53	1.05	0.31	-	0.08	15.17	-	96.60

altered, silicified rocks (sample A23). These oxides consist of fine-grained aggregates of **hematite**, **magnetite** and/or **magnesiochromite** accompanied by minute **sulphide** minerals or veinlets where **todorokite** is present in very fine veinlets.

Table 4 Representative microprobe analysis of carbonated-fluorapatite (A8 sample).

	1	2	3	4	5	6
P_2O_5	37.11	37.32	37.89	37.93	38.27	38.58
CaO	53.79	53.55	54.79	53.98	53.50	54.36
F	3.09	3.32	2.19	3.09	3.33	2.91
MnO	1.56	1.36	1.57	1.44	1.41	1.54
SiO_2	1.53	0.79	2.13	1.44	1.07	0.20
Σ	96.98	96.34	98.57	97.88	97.58	97.59

Some siliceous concretions are equally related to **hematite**, **goethite** and **todorokite** veinlets and are crosscut by chalcedony veinlets (samples A71, B15 and B16) being similar and analogous to hematite-rich nodular concretions found southward and in proximity to the Taxiarches Monastery Fe-Cu-stockwork mineralization (Photiades, 1986).

Table 5. Representative microprobe analyses of todorokite (1-3) associated with cryptomelane (4-5) in fine veinlets (B8 sample)

	1	2	3	4	5
MnO_2	77.22	79.06	79.58	89.90	90.21
Fe_2O_3	0.22	0.29	0.34	0.20	0.23
TiO_2	0.03	-	-	0.07	0.09
CaO	4.91	3.65	2.91	0.85	0.98
MgO	0.74	1.67	2.53	0.15	0.11
CuO	0.38	0.18	-	-	-
SiO_2	1.52	0.02	0.30	0.22	0.12
K_2O	0.84	0.44	0.72	4.60	4.09
Na_2O	-	-	-	-	-
BaO	2.39	2.46	0.94	-	-
SrO	0.07	0.07	0.04	0.27	0.22
H_2O	11.92	11.74	11.87		
Σ	100.24	99.58	99.23	96.26	96.05

Moreover, magnetite in these nodular concretions contains up to 1% manganese and inclusions of Ag-bearing **millerite** (Tab. 6) and **pyrite**. Magnetite occurs as minute lamellae, slightly deformed, and altered into martite (sample 655, Fig. 6A).

Todorokite veinlets are most abundant in red jasper and chert concretions; they are similar in composition and textural structure to todorokite in the friable Mn concretions. However, todorokite in the compact concretions has progressively high crystallinity in comparison to that of the friable concretions, so a large amount of this mineral is easily observable under the microscope and in XRD films. Microprobe analyses (Tab. 7) reveal a significant substitution of manganese for iron and enrichment in trace elements (Tab. 8). Radiolarians in cherts, closest to the todorokite veinlets have been alterated epigenetically to todorokite (Fig. 6B).

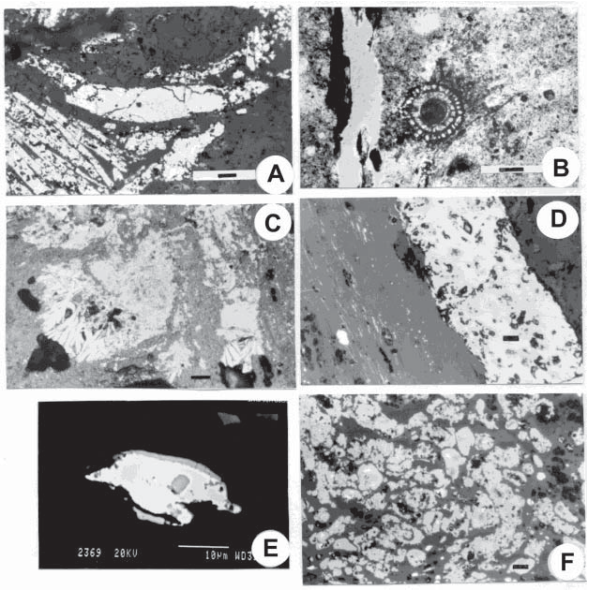

Fig. 6. Various minerals in compact concretions. **A:** Lamellated magnetite slightly converted into martite. (655 sample, natural reflected light scale 30 μm); **B:** radiolarians of red-jasper have undergone epigenetic transformations into todorokite (natural transmitted light scale 30 μm); **C:** Fine Mn-concretions and veinlets of Ni-rich todorokite with numerous scattered droplets of pyrite and millerite (A23 sample, reflected light, scale 30 μm); **D:** Alignment of very fine grains of native copper and cuprite neighboring a cuprite veinlet (A3 sample, reflected light, scale 40 μm); **E:** Minute native copper grain as droplet (white) surrounded by covellite (grey) (A3 sample, Back-scattered electron image); **F:** Elongated cuprite grains carry native copper inclusions (A3 sample, reflected light, scale 40 μm).

Table 6. Representative microprobe analysis of millerite (A23 sample).

	S	Ni	As	Mn	Fe	Bi	Ag	Co	Sb	Cu	Zn	Au
1	34.29	61.39	-	-	2.64	-	**0.26**	0.02	0.14	0.29	0.24	-
2	34.68	61.34	-	-	0.73	-	**0.25**	0.13	-	0.19	0.30	-
3	35.01	62.25	-	0.13	0.51	-	**0.17**	0.07	0.01	-	0.14	-

Coarse-grained magnesiochromite crystals occur in compact concretions of highly alterated /silicified serpentinite, and are cemented by chalcedony and carbonates. The carbonate minerals consist of **manganiferous calcite** and **kutnahorite** (MnO = 12-15%, CaO = 29-35%, MgO = 1.4-3%, FeO = 2-3%) that underline a late re-deposition of manganese. Magnesiochromite is associated with fine-veinlets and disseminated grains of sulphides and with concretionary fine-grained manganese and Mn-veinlets.

Table 7. Representative microprobe analysis of todorokite (A18 sample).

	1	2	3	4
MnO_2	74.48	79.32	79.46	80.38
CaO	2.63	2.80	2.78	2.90
MgO	1.39	1.47	2.17	1.44
Fe_2O_3	4.28	0.42	0.79	0.33
BaO	2.01	2.45	2.17	1.16
K_2O	0.62	0.61	0.67	0.78
H_2O	11.47	11.82	11.86	11.87
Σ	96.88	98.89	99.90	98.96

Microprobe analyses show zoned magnesiochromite, with higher chrome content in the cores and replacement of chrome by aluminum and magnesium towards the rims (Tab. 9, columns 1 to 3). Nickel-rich serpentine fragments (1-2 % NiO) adhere to the rims. Co-existing sulphides consist of millerite and pyrite, whereas the concretionary fine-grained manganese and Mn-veinlets (Fig. 6C) are composed of Ni-rich todorokite with Ni content higher than 10 wt% (Photiades et al., 1995). These manganese oxides reveal relatively high contents of nickel, iron, and cobalt (Tab. 10).

Table 8. Representative microprobe analysis of todorokite trace elements (A18 sample).

	As	Sb	Co	Cu	Ni	Pb	Zn
1	243	248	18	135	341	698	10
2	235	340	28	170	397	691	140
3	232	138	34	157	644	695	165
4	236	186	86	45	388	474	259
5	234	146	86	39	352	677	219

Deformed basalt fragments are also shaped comparable to compact nodular concretions. These basalts (Fig. 4D, sample A3) include aligned **native copper**, **cuprite** (Cu_2O), **chalcocite** (Cu_2S), and **algodonite** ($Cu_{6\text{-}7}As$), a copper arsenide, and impregnated by copper carbonate hydroxides like **azurite** $[Cu_3(CO_3)_2(OH)_2]$ and **malachite** $[Cu_2(CO_3)(OH)_2]$.

Table 9. Representative microprobe analysis of magnesiochromite (A23 sample).

	Cr_2O_3	Al_2O_3	FeO	Fe_2O_3	MgO	MnO	CaO	TiO_2	SiO_2	Σ
1	53.39	10.60	19.44	4.37	7.91	0.50	0.29	0.19	0.13	96.82
2	47.79	17.47	18.50	4.46	10.09	0.39	-	0.15	0.20	99.05
3	42.55	21.67	14.87	5.89	12.69	0.34	0.03	0.16	0.18	98.28

The native copper forms mainly well elongated and equally an oriented crystal with algodonite microscopically rims (Tab. 11).

Table 10. Representative microprobe analysis of todorokite (A23 sample).

	MnO_2	CaO	MgO	NiO	CoO	Fe_2O_3
1	66.25	1.32	0.56	12.14	0.27	1.24
2	68.78	0.63	0.18	10.36	0.13	1.27
3	70.31	1.16	0.10	10.08	0.55	0.93
4	71.31	1.29	0.31	9.34	0.59	1.11
5	72.86	1.66	0.64	8.05	0.28	0.47
6	74.92	2.01	0.79	6.92	0.06	0.36

Besides, the trace elements in the present **chalcocite** include As, Au, Co, Sb, and Zn (Tab. 12)**.** Cuprite occurs as millimeter-sized veinlets (Fig. 6D) and with chalcocite also occurring as lamellae or elongated grains and replacing the native copper that appears as abundant inclusions (Fig. 6E, F).

Table 11 Representative microprobe analysis of algodonite (A3 sample).

	As	Cu	Mn	Fe	Bi	Ag	Co	Sb	Ni	Zn	Au
1	**14.32**	**86.16**	0.06	0.01	-	0.07	0.04	-	-	0.18	-
2	**14.65**	**84.31**	0.06	0.07	0.01	0.26	0.03	-	-	-	0.03
3	**15.06**	**84.32**	-	0.08	-	-	0.14	0.06	-	-	0.24
4	**15.17**	**84.32**	0.06	0.03	0.25	0.08	-	0.01	0.11	0;07	-
5	**15.87**	**82.26**	0.09	-	-	0.06	0.06	-	-	-	-
6	**16.02**	**83.13**	-	0.02	-	-	0.05	0.13	-	0.03	-
7	**16.58**	**83.02**	0.03	-	0.12	-	0.06	-	0.03	0.41	-
8	**17.08**	**83.54**	-	-	-	0.06	0.06	0.03	0.08	-	-
9	**21.10**	**78.06**	-	-	0.03	0.12	-	0.15	-	0.30	0.20

Paragenetic mineralogical order of compact Fe-Mn concretions is characterized by magnetite and by sulphide (millerite, pyrite, algodonite, chalcocite) mineralizations and pass up successively into hematite and native copper and then into copper oxidized minerals, like cuprite and the whole assemblage is crosscut by highly crystallized todorokite veinlets, chalcedony and various carbonates.

Table 12. Representative microprobe analysis of chalcocite (A3 sample).

	S	Cu	As	Mn	Fe	Bi	Ag	Co	Sb	Ni	Zn	Au
1	**19.90**	**78.49**	0.02	0.15	0.09	-	-	-	0.09	-	0.21	0.07
2	**20.05**	**77.89**	-	-	0.03	0.05	-	-	-	0.17	0.29	-
3	**20.16**	**78.09**	-	0.16	0.03	0.26	0.09	-	-	-	0.30	0.13
4	**20.23**	**78.98**	0.40	-	0.04	-	-	-	-	0.18	0.08	-
5	**20.25**	**79.34**	-	0.09	0.05	0.07	0.14	0.03	-	0.03	-	0.03
6	**20.28**	**79.24**	0.06	0.11	0.01	0.11	0.09	-	-	-	0.11	-
7	**20.29**	**79.81**	0.03	0.03	0.09	0.06	-	0.05	-	-	-	-
8	**20.34**	**80.08**	-	-	0.04	-	-	0.05	0.20	0.04	0.20	-
9	**20.40**	**79.74**	-	0.11	0.01	-	-	0.02	-	-	-	0.15
10	**20.59**	**79.96**	0.02	0.04	0.08	-	-	-	0.02	-	0.03	-
11	**20.80**	**78.36**	0.07	-	0.06	-	-	-	0.05	-	-	0.06
12	**20.85**	**77.17**	0.14	0.05	0.05	0.01	0.26	0.03	-	-	-	-

6. Chemistry

Samples under study (Tab. 13, A4, A22, A70, A72 and B9) contain high percentage of Mn and low percentage in Fe and in Ni, Co and Cu and appear to be in good agreement with microprobe analyses of oxide minerals related to these friable concretions, which are also characterized by high in Mn, and low in Fe and transition metals. These elements are a tool to be presented as a model for describing the type of mineralization and development of manganese mineral types. The plot of Fe, Mn, and (Ni+Co+Cu) x10 (Bonatti et al., 1972**)** clearly reveals that the origin of the iron and the manganese of nodular friable concretions of the area is due to hydrothermal activity (Fig. 7).

Table 13. Chemical analysis of selected samples of the friable and compact concretions from Angelokastron and Lykotroupi, Argolis.

	A4	A22	A70	A72	B9	A71	B15	B16
Si wt%	28.89	22.26	19.82	9.06	24.29	7.59	8.28	6.35
Mn	13.32	13.4	22.25	32.50	22.49	20.95	20.10	23.83
Fe	1.75	2.31	2.41	1.82	0.45	17.64	20.05	23.31
Al	0.82	0.87	1.19	0.13	0.32	0.77	0.77	0.77
Ni ppm	300	240	280	340	300	340	320	320
Co	300	240	300	320	360	380	320	320
Cu	200	100	180	300	140	160	80	160

Besides, the distribution of a few selected samples from compact concretions (Tab. 13, B15, B16 and A71) appears to have an equal percentage of Mn and Fe-oxides. With those percentages, they enter into the hydrothermal field (Fig. 7) and more precisely, approach the hydrothermal sector limited by notronites of Aden Gulf (Cann et al., 1977).

The study of friable nodular concretions show Mn rich hydrothermal end members, which are characteristic of hydrothermal Mn-ore deposits like Epidavros (Photiades, 1986; Wackenheim et al., 1987), Apennine (Bonatti et al., 1976), Alpine-type (Peters, 1988; Perseil and Latouche, 1989), Oman (Peters, 1988), Franciscan (Crerar et al., 1982) and Tokoro deposits (Choi and Hariya, 1990).

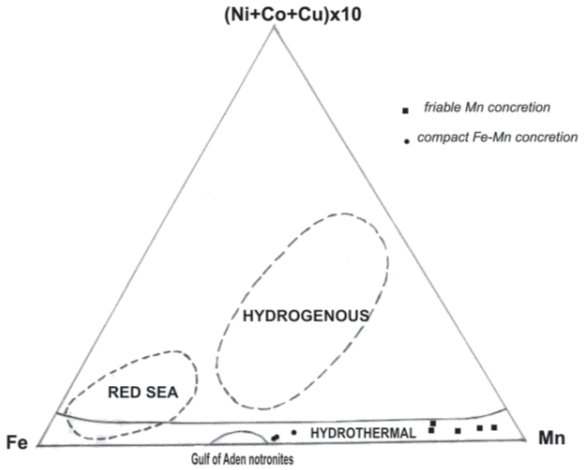

Fig. 7. Ternary diagram (Ni+Co+Cu)x10-Fe-Mn (from Bonatti et al., 1972) with notronites of Aden Gulf (Cann et al., 1977) showing the hydrothermal origin of the Argolis friable and compact concretions.

Furthermore, the low Si/Al ratio (Fig. 8) was also used to emphasize the hydrothermal source (Crerar et al., 1982) of the examined friable and compact nodular concretions.

7. Discussion-Conclusion

Argolis Fe-Mn nodular concretions fail to demonstrate the typical botryoidal internal manganese microstructure patterns, which characterize the modern nodules (Sorem and Fewkes, 1977, Halbach and Ozkara, 1979). They also differ from fossil nodules that preserve a botryoidal internal manganese structure as described in the Swiss Alps (Perseil and Latouche, 1989), and Costa Rica (Kuypers and Denyer, 1979; Halbach et al., 1992). Likewise, the studied concretions fail to show Mn-

microstructures similar to those of ferromanganiferous crusts, precipitated on some modern oceanic basalts (Toth, 1980).

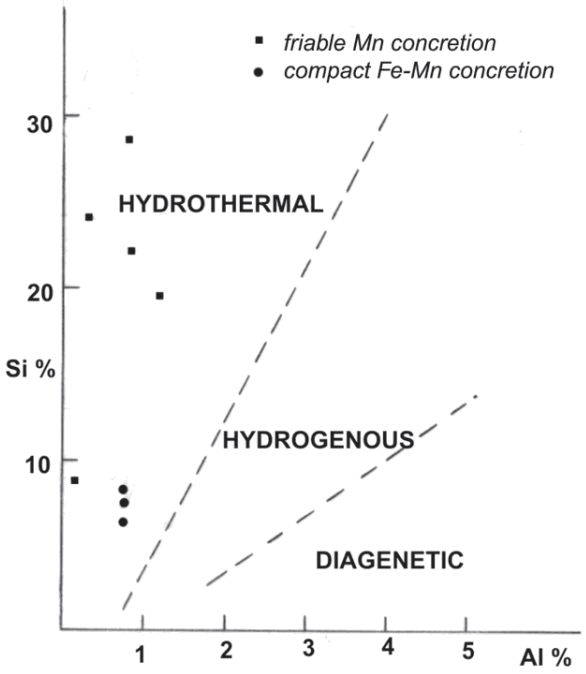

Fig. 8. Si/Al diagram (from Crerar et al., 1982) showing the hydrothermal origin of the Argolis friable and compact concretions.

Furthermore, the observed todorokite as sheaf-like texture is completely lacking from modern deep-see manganese minerals (Perseil and Jehanno, 1981). In addition, the occurrence of birnessite is very rare in the deep-sea manganese nodules (Usui, 1986). Moreover, the presence of pyrolusite as a matrix further differentiates our concretions from those of the modern deep-sea environment.

The friable Mn concretions are characterized by late-stage hydrothermal solutions that have penetrated the various siliceous concretions leaving behind cryptomelane, todorokite and manganite that gives rise to pyrolusite. These oxides occur within the jaspers and in association with boxwork vein systems of hollandite, birnessite to nsutite and by the youngest generation of manganiferous carbonated-fluorapatite and carbonates.

Cryptomelane, as the main mineral reflects the relatively low temperature environment of mineralization rich in ions of K and Si and occurs in variable environments of weathering i.e. a phase of active leaching of basaltic rocks in low temperature conditions (Photiades and Economou, 1991; Perseil and Photiades, 1993).

The studied hollandite series show enrichment of Ba, are free of Fe, revealing their chemical environment of formation. The hollandite mineral, free of Fe, can form when Fe would be leached out, due to a drop in pH, in which K becomes active with Ba to take part first in the formation of cryptomelane and later of hollandite, because the accommodation of the larger cations depends on the temperature and the environment of formation (Burns and Burns, 1977).

However, the presence of todorokite and birnessite appears when an oxidizing, low alkalinity, with active hydration and a relatively low temperature environment is dominant, giving rise to these hydrothermal minerals, accreted at the sea floor near fumarolic hot springs during volcanic activity, like the Cuban Eocene Mn deposit (Burns at al., 1983).

Maybe the association of manganite and pyrolusite is an indicator of low temperature hydrothermal alteration in an oxidizing alkaline environment, because pyrolusite is also formed when epithermal solutions containing manganese meet oxygenated water in a pH range of 8 to 9. Most probably, it was a period of relative calmness and chemical weathering taking place at low temperatures over the sea bottom with an 8-9 pH range.

However, the carbonate-fluorapatite into Ca-rich cryptomelane, associated with pyrolusite, is connected with subsequently more oxidized hydrothermal conditions (Perseil et al., 1995).

On the other hand, the compact Fe-Mn concretions are highly heterogeneous and are characterized by sulphide (millerite, pyrite, algodonite, chalcocite) and iron oxide (magnetite) mineralizations and pass up successively into hydrous ferric oxide (hematite, goethite) and native copper and then into copper oxidized minerals (cuprite). On that substratum, the highly crystallized, iron rich todorokite is generated. Besides, the Ni-rich todorokite in fissures as well as the chalcedony veins, are also following a hydrothermal contribution (Photiades et al., 1995).

Additionally, the precipitation of the hydrous ferric oxide (goethite and hematite) and the manganese oxides require a chemical environment with oxidizing conditions. However, manganese oxides precipitate at a slightly higher pH than hydrous ferric oxide (Stumm and Morgan, 1970). This chemical gradient implies the presence of a variable pH during the formation of the compact nodular concretions that are equally rich firstly in Fe and then in Mn mineralization.

It is clear that the examined iron-manganese concretions are of hydrothermal origin and differ substantially from those of typical deep-sea hydrogenous Mn deposits. The above hypothesis also gets support from the mineralogical and chemical data already described which are similar to those of hydrothermal origin from active mid-oceanic ridges (Cronan, 1977).

The iron-manganese concretions result from submarine hydrothermal activity associated with an intense fissural process that increases the permeability of the rocks and provides conduits for hydrothermal solutions. These processes would have taken place during the pre-emplacement period of the Neotethyan oceanic crust preserved as a Subpelagonian ophiolite.

Acknowledgments

I would like to thank the Museum National d' Histoire Naturelle of Paris which hosted me during the preparation of this work.

References

Badia D. and Frohlich F., 1975. Identification de la chalcedoine par son spectre infrarouge. C. R. Acad. Sci., 281, 85-88.

Baumgartner P.O., 1985. Jurassic sedimentary evolution and nappe emplacement in the Argolis Peninsula (Peloponnesus; Greece). Mem. Soc. Helv. Sci. Nat. 99, 111 pp.

Bonatti E., Kraemer T. and Rydell H., 1972. Classification and genesis of submarine iron-manganese deposits. In: Horn, D.R. (ed.), Ferromanganese deposits on the ocean floor: International Decade on Ocean Exploration, Nat. Sci. Found., Washington D.C., 149-166.

Bonatti E., Zerbi M., Kay R. and Rydell H., 1976. Metalliferous deposits from the Apennine ophiolites: Mesozoic equivalents of modern deposits from oceanic spreading centers. Geol. Soc. Am. Bulletin, 87, 83-94.

Bortolotti V., Chiari M., Marcucci M., Photiades A. and Principi G., 2001. Triassic radiolarian assemblages from the cherts associated with pillow lavas in Argolis Peninsula (Greece). Ofioliti, vol. 26/1, p. 75.

Bortolotti V., Carras N, Chiari M., Fazzuoli M., Marcucci M., Photiades A. and Principi G., 2002. New geological observations and biostratigraphic data on the Argolis Peninsula: palaeogeographic and geodynamic implications. Ofioliti 27, 43-46.

Bortolotti V., Carras N, Chiari M., Fazzuoli M., Marcucci M., Photiades A. and Principi G., 2003. The Argolis Peninsula in the palaeogeographic and geodynamic frame of the Hellenides. Ofioliti, 28/2, 79-94.

Burns R.G. and Burns V.M., 1977. Mineralogy, in Marine manganese deposits G.P. Glasby ed. Elsevier Sci. Pub. Co. Amsterdam, pp. 185-248.

Burns R.G., Burns V.M. and Stockman H.W., 1983. A review of the todorokite-buserite problem: implications to the mineralogy of marine manganese nodules, Am. Min. v. 68, pp. 972-980

Cann J.R., Winter C.K. and Pritchard R.G., 1977. A hydrothermal deposit from the floor of the Gulf of Aden. Mineralogical Magazine, 41, 193-199.

Capedri S., Grandi R., Photiades A. and Toscani L., 1996. "Boninitic" clasts from the Mesozoic olistostrome and turbidites of Angelokastron (Argolis, Greece). Geological Journal, vol. 31, 301-322.

Chiari M., Baumgartner P.O., Bernoulli D., Bortolotti V., Marcucci M., Photiades A. and Principi G., 2003. Radiolarians document the reworking of early Jurassic manganese nodules in a Middle Jurassic oceanic mélange, Angelokastron, Argolis Peninsula, Eastern Greece. Abstracts and Programme in 10th INTERRAD (Tenth meeting of the International Association of Radiolarian Paleontologists), Univ. of Lausanne, Sept. 7-12 2003, Switzerland, pp. 40-41.

Chiari M., Baumgartner P.O., Bortolotti V., Bernoulli D., Marcucci M., Photiades A. and Principi G., 2004a. Early Jurassic radiolarians from reworked manganese nodules in a Middle Jurassic oceanic melange, Argolis peninsula (Greece). 32nd IGC - Florence, 2004, "Radiolaria and radiolarites in orogenic belts", 60-3, p. 299.

Chiari M., Baumgartner P.O., Bernoulli D., Bortolotti V., Marcucci M., Photiades A. and Principi G., 2006. Jurassic radiolarians from reworked manganese nodules in an oceanic mélange, Argolis Peninsula (Greece). Abstracts of Talks and Posters presented during the 7th International Congress on the Jurassic System, September 6-18, 2006, Krakow, Poland, Volumina Jurassica, Volumen IV, p.*40.*

Chiari M., Bortolotti V., Marcucci M., Photiades A. and Principi G., 2004b. New biostratigraphic data from the radiolarian cherts associated with pillow lavas in the Argolis peninsula (Greece) 32nd IGC - Florence, 2004, "Radiolaria and radiolarites in orogenic belts", 60-8, p. 300-301.

Chiarri M., Bortolotti V., Marcucci M., Photiades A. and Principi G., 2007. Datings of the cherts associated with basalts in the Argolis Peninsula (Greece). Abstract p.135, T18-14, Epitome vol.2, 2007*, Geoitalia 2007, FIST, Rimini, 12-14 settembre 2007.*

Choi J.H. and Hariya Y., 1990. Trace element concentration of manganese deposits in the Tokoro Belt, Hokkaido, Japan. Jour. Fac. Sci. Hakkaido Univ. Ser IV, 22, 553-564.

Crerar D.A., Namson J., Chyi M.S., William L. and Feigenson M.D., 1982. Manganiferous chert of the Franciscan Assemblage: General Geology, ancient and modern analogues, and implications for hydrothermal connection at oceanic spreading centers. Econ. Geol., 77, 519-540.

Cronan D.S., 1980. Underwater minerals, 361p. Academic Press, London.

Dostal J., Toscani L., Photiades A. and Capedri S., 1991. Geochemistry and petrogenesis of Tethyan ophiolites from northern Argolis (Peloponnesus, Greece). Eur. J. Mineral., 3, 105-121.

Halbach P. and Ozkara M., 1979. Morphological and geochemical classification of deep-sea ferromanganese nodules and its genetical interpretation. Colloques Internationaux du C.N.R.S. N° 289-La Genese Des Nodules De Manganese, 77-88.

Halbach P., Gursky H.J., Gursky M.M., Schmidt-Effing R. and Maresch W.V., 1992. Composition and formation of fossil manganese nodules in Jurassic to Cretaceous radiolarites from the Nicoya Ophiolite Complex (NW Costa Rica). Mineral. Deposita, 27, 153-160.

Perseil E.A. and Jehanno C., 1981. Sur les caracteres mineralogiques et geochimiques des nodules polymetalliques du Bassin Indien Central. Mineral. Deposita, 16, 391-407.

Perseil E. A. and Latouche L., 1989. Decouverte de microstructures de nodules polymetalliques dans les mineralisations manganesiferes metamorphiques de Falotta et de Parsettens (Grisons-Suisse). Mineral. Deposita, 24, 111-116.

Perseil E.A. and Photiades A., 1993. Les mineralisations manganesiferes a macfallite et orientite de l' Argolide septentrionale (Grece). Mineralogie et metallogenie. Bull. Mus. natl. Hist. nat., Paris, 4e ser., 15, section C, N° 1-4, 3-24.

Perseil E.A., Photiades A.D. and Giovanoli R., 1998. Manganiferous concretions bearing luminescent fluorapatite in Jurassic red cherts of pillow-lavas ophiolite unit (Angelokastro, Argolis). *Proceedings of 8th International Congress, Patras, May 1998. Bull. Geol. Soc. Greece, vol. XXXII/3, 13-19.*

Peters Tj., 1988. Geochemistry of manganese-bearing cherts associated with Alpine ophiolites and the Hawasina formation in Oman. Marine Geol., 84, 229-238.

Photiades A.D., 1986. Contribution à l'étude géologique et métallogénique des unités ophiolitiques de l'Argolide septentrionale (Grèce). *Thèse de Doctorat de 3e cycle, Université de Franche - Comté (Besançon), n0 499, 261 p.*

Photiades A. and Economou G., 1991. Alteration hydrothermale sous-marine des basaltes et des dolerites (facies zeolitique) de l' unite moyenne "volcanique" de l' Argolide septentrionale (Peloponnese, Grece). Bull. Geol. Soc. Greece, 25/2, 301-319.

Photiades A.D., Perseil E.A. and Meisser N., 1995. A Ni - rich todorokite from the Middle volcanic ophiolitic unit of Northern Argolis (Greece*). Geol. Soc. Greece, Sp. Pub. No 4/2, 467-471.*

Saccani E., Padoa E. and Photiades A., 2003. Triassic mid-ocean ridge basalts from the Argolis Peninsula (Greece): new constraints for the early oceanization phases of the Neo-Tethyan Pindos basin. *In: Dilek Y. and Robinson P.T. (Eds.) "Ophiolites in Earth History", Geol. Soc. London Sp. Publ., 218, 109-127.*

Sorem R.K. and Fewkes R.H., 1977. Internal characteristics; In: Marine Manganese (edit. G.P. Glasby) Elsevier Oceanography series., 147-183.

Stumm W. and Morgan J.J., 1970. Aquatic Chemistry. Wiley Inter-science, New York, 583p.

Toth J.R., 1980. Deposition of submarine crusts in manganese and iron. Geol. Soc. Am. Bull. Part 1, 91, 44-54.

Usui A., 1986. XIV. Mineralogy and internal structure of manganese nodules in the GH81-4 area. Geol. Surv. Japan Cruise Report, No, 21, p.219-230.

Wackenheim C., Photiades A. and Thiebaut J., 1987. Les mineralisations manganesiferes associees aux basaltes ophiolitiques de la region d'Epidaure (Argolide septentrionale, Grece). *C. R. Acad. Sci. Paris, 305, serie ll, 1445-1448.*